

## A FRACTIONAL STEP IMMERSED BOUNDARY METHOD FOR STOKES FLOW WITH AN INEXTENSIBLE INTERFACE ENCLOSING A SOLID PARTICLE\*

MING-CHIH LAI<sup>†</sup>, WEI-FAN HU<sup>‡</sup>, AND WEN-WEI LIN<sup>‡</sup>

**Abstract.** In this paper, we develop a fractional step method based on the immersed boundary (IB) formulation for Stokes flow with an inextensible (incompressible) interface enclosing a solid particle. In addition to solving for the fluid variables such as the velocity and pressure, the present problem involves finding an extra unknown elastic tension such that the surface divergence of the velocity is zero along the interface, and an extra unknown particle surface force such that the velocity satisfies the no-slip boundary condition along the particle surface. While the interface moves with local fluid velocity, the enclosed particle hereby undergoes a rigid body motion, and the system is closed by the force-free and torque-free conditions along the particle surface. The equations are then discretized by standard centered difference schemes on a staggered grid, and the interactions between the interface and particle with the fluid are discretized using a discrete delta function as in the IB method. The resultant linear system of equations is symmetric and can be solved by fractional steps so that only fast Poisson solvers are involved. The present method can be extended to Navier–Stokes flow with moderate Reynolds number by treating the nonlinear advection terms explicitly for the time integration. The convergent tests for a Stokes solver with or without an inextensible interface are performed and confirm the desired accuracy. The tank-treading to tumbling motion for an inextensible interface enclosing a solid particle with different filling fractions under a simple shear flow has been studied extensively, and the results here are in good agreement with those obtained in literature.

**Key words.** immersed boundary method, inextensible interface, solid particle, fractional step method, Stokes flow

**AMS subject classifications.** 65M06, 76D07

**DOI.** 10.1137/100818777

**1. Introduction.** Most biological cells consist of a lipid bilayer membrane encapsulating the cellular content. For instance, a human leukocyte contain a nucleus occupying 18%–44% of the volume [21], which affects the cell adhesion during inflammatory responses. It is important to study the dynamics of a compound vesicle (a lipid bilayer membrane enclosing a fluid with a suspended particle) [26]. For simplicity, we regard the lipid bilayer membrane as an inextensible interface. Thus, in this paper, we develop a fractional step method based on the immersed boundary (IB) formulation for Stokes flow with an inextensible (incompressible) interface enclosing a solid particle.

Most previous studies in the literature have focused on an inextensible interface enclosing a homogeneous fluid. Even in that case, there are still some numerical issues to be addressed. In addition to solving for the fluid variables such as the velocity and pressure, the above problem involves finding extra unknown elastic tension such that the surface divergence of the velocity is zero along the interface. Once the velocity

---

\*Submitted to the journal's Computational Methods in Science and Engineering Section December 20, 2010; accepted for publication (in revised form) August 22, 2012; published electronically DATE.  
<http://www.siam.org/journals/sisc/x-x/81877.html>

<sup>†</sup>Corresponding author. Center of Mathematical Modeling and Scientific Computing & Department of Applied Mathematics, National Chiao Tung University, 1001, Ta Hsueh Road, Hsinchu 300, Taiwan (mclai@math.nctu.edu.tw). This author's work was supported in part by National Science Council of Taiwan under research grant NSC-98-2115-M-009-014-MY3, and by the NCTS in Taiwan.

<sup>‡</sup>Department of Applied Mathematics, National Chiao Tung University, 1001, Ta Hsueh Road, Hsinchu 300, Taiwan (weifanhu.am95g@g2.nctu.edu.tw, wwlin@math.nctu.edu.tw).

is found, the interface moves according to the local fluid velocity as usual. Since the interface is inextensible, the total length of the interface should be conserved. This mathematical model is motivated by the simulation of vesicle dynamics [10], and the deformation of erythrocytes [14, 17] and drug-carrying capsules [20], just to name a few. In particular, the dynamics of moving vesicles have been extensively explored both experimentally [6, 9] (see also and the references therein) and computationally [10, 28, 25, 22, 7, 11]. Notice that the dynamics of vesicles are determined by their boundary rigidity, inextensibility, and the hydrodynamical forces.

In previous literature, most related work is based on boundary integral methods; see, for example, [28, 25, 22] and the references therein. However, boundary integral methods generally assume infinite domains and cannot be generalized to full Navier–Stokes equations since there is no corresponding Green function. Until recently, Kim and Lai [7] applied a penalty IB method to simulate the dynamics of inextensible vesicles. By introducing two different kinds of Lagrangian markers, the authors are able to decouple the fluid and vesicle dynamics so that the computation can be performed more efficiently. One potential problem with this approach is that the time step depends on the penalty numbers and must be chosen smaller as the penalty number becomes larger. In [11], a new finite difference scheme based on the immersed interface method (IIM) has been developed for solving the present problem in Navier–Stokes flow. The authors treat the unknown elastic tension as an augmented variable so that the augmented IIM can be applied.

We summarize the contributions of the present work as follows:

- We develop a linearly semi-implicit scheme (section 3) for the model of Stokes flow with an inextensible interface enclosing a solid particle, which has potential applications to the dynamics of a compound vesicle and is less investigated in the literature. The present scheme can be extended to Navier–Stokes flow with moderate Reynolds number by treating the nonlinear advection terms explicitly.
- We show that the spreading operator of the tension and the surface divergence operator of the velocity are skew-adjoint mathematically (section 2). This skew-adjoint property is also preserved in the discrete form (section 4.1), which makes the resultant linear system symmetric (section 4.1 and also Appendix B). A fractional step method that exploits fast Poisson solvers can be efficiently applied to solving the linear system (section 4.3).
- Unlike our previous work using a penalty approach [7], here we are able to estimate the local error of inextensibility for two successive time steps (see (21) in section 3). In addition, there are no penalty parameters introduced as in [7], so the time step size can be significantly increased (see the time step chosen in section 5.2). From those points of view, the present scheme does offer significant improvements or the accuracy and stability achieved in the previous work.
- We present numerical results (section 5) of the tank-treading to tumbling motions for an inextensible interface enclosing a solid particle with different filling fractions under shear flow. We have found that, by the increase of the filling fraction, the interface tends to transit from tank-treading to tumbling (section 5.3). We also compute the critical filling fractions for different reduced areas (section 5.3), and the results are qualitatively consistent with those in [26].

The rest of the paper is organized as follows. In the next section, we describe our governing equations for the Stokes flow with an inextensible interface enclosing

a suspended solid particle based on an IB formulation. We also show the skew-adjoint property between the spreading operator acting on the tension and the surface divergence operator acting on the velocity. In section 3, we discretize the governing equations by centered difference schemes on a staggered grid. Some implementation details including the proof of the symmetric property of the resultant matrix and the existence of a solution in the linear system, and the fractional step method for solving the resultant linear system are all given in section 4. Numerical results including the convergence and efficiency tests and the simulations for tank-treading to tumbling motion with different filling fractions for the present model are shown in section 5. Some conclusions are given in section 6.

**2. Governing equations.** Consider a moving, immersed, inextensible interface  $\Gamma$  enclosing a suspended solid particle  $P$  in a two-dimensional fluid domain  $\Omega$ , as shown in Figure 2.1. We assume that the fluids inside and outside of the interface are the same and governed by the incompressible Stokes equations, and the particle's gravity is neglected. Using the IB formulation of the model [16, 7], the inextensible interface and the solid particle surface are regarded as singular force generators in the fluid equations. Let us describe the inextensible interface  $\Gamma$  and the particle surface  $\partial P$  by parametric forms  $\mathbf{X}(s, t) = (X_1(s, t), X_2(s, t))$  and  $\mathbf{Y}(\alpha, t) = (Y_1(\alpha, t), Y_2(\alpha, t))$ , respectively, where  $s$  and  $\alpha$  are the corresponding Lagrangian parameters. The governing equations in dimensionless form can be written as follows:

$$(2.1) \quad -\nabla p + \Delta \mathbf{u} + \int_{\Gamma} \frac{\partial}{\partial s} (\sigma \boldsymbol{\tau}) \delta(\mathbf{x} - \mathbf{X}(s, t)) \, ds + \int_{\partial P} \mathbf{F}(\alpha, t) \delta(\mathbf{x} - \mathbf{Y}(\alpha, t)) \, d\alpha = 0 \quad \text{in } \Omega,$$

$$(2.2) \quad \nabla \cdot \mathbf{u} = 0 \quad \text{in } \Omega,$$

$$(2.3) \quad \nabla_s \cdot \mathbf{U} = \frac{\partial \mathbf{U}}{\partial s} \cdot \frac{\boldsymbol{\tau}}{|\frac{\partial \mathbf{X}}{\partial s}|} = 0 \quad \text{on } \Gamma,$$

$$(2.4) \quad \mathbf{U}(s, t) = \int_{\Omega} \mathbf{u}(\mathbf{x}, t) \delta(\mathbf{x} - \mathbf{X}(s, t)) \, d\mathbf{x}, \quad \frac{\partial \mathbf{X}}{\partial t}(s, t) = \mathbf{U}(s, t) \quad \text{on } \Gamma,$$

$$(2.5) \quad \mathbf{V}(\alpha, t) = \int_{\Omega} \mathbf{u}(\mathbf{x}, t) \delta(\mathbf{x} - \mathbf{Y}(\alpha, t)) \, d\mathbf{x} = \mathbf{V}_c(t) + \omega(t) \begin{bmatrix} -(Y_2(\alpha, t) - Y_{2c}(t)) \\ Y_1(\alpha, t) - Y_{1c}(t) \end{bmatrix} \quad \text{on } \partial P,$$

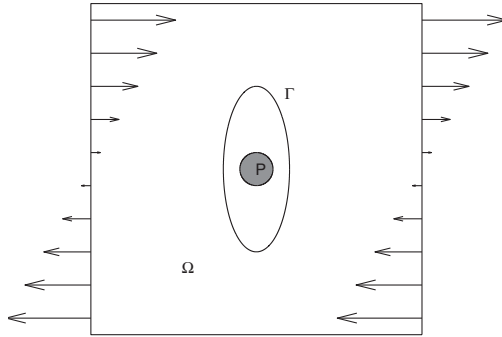


FIG. 2.1. A diagram of an inextensible interface enclosing a solid particle in a shear flow.

$$(2.6) \quad \int_{\partial P} \mathbf{F}(\alpha, t) \, d\alpha = 0, \quad \text{where } \mathbf{F}(\alpha, t) = (F_1(\alpha, t), F_2(\alpha, t)),$$

$$(2.7) \quad \int_{\partial P} F_1(\alpha, t) (Y_2(\alpha, t) - Y_{2c}(t)) - F_2(\alpha, t) (Y_1(\alpha, t) - Y_{1c}(t)) \, d\alpha = 0.$$

Equations (2.1) and (2.2) are the familiar incompressible Stokes equations with singular force terms arising from the inextensible interface and the particle surface. Here,  $\mathbf{u} = (u, v)$  and  $p$  are the velocity field and the pressure, both described in Cartesian coordinates. Equation (2.3) represents the inextensibility constraint of the interface which is equivalent to the zero surface divergence of the velocity along the interface due to the fact that the local stretching factor [13],

$$\frac{\partial}{\partial t} \left| \frac{\partial \mathbf{X}}{\partial s} \right| = (\nabla_s \cdot \mathbf{U}) \left| \frac{\partial \mathbf{X}}{\partial s} \right| \quad \text{on } \Gamma,$$

must be zero along the interface. Equation (2.4) simply states that the interface moves along with the fluid and that the velocity  $\mathbf{U}$  is the interpolation of the fluid velocity at the interface. The interaction between the fluid and the interface or the particle is linked by the two-dimensional Dirac delta function  $\delta(\mathbf{x}) = \delta(x)\delta(y)$ .

Since the particle behaves like a rigid body, its motion is governed by the translational and rotational velocities around the center of the particle. Moreover, the velocity of the particle surface must equal the fluid velocity (no-slip boundary condition). Equation (2.5) describes the particle surface velocity in which  $\mathbf{V}_c(t)$  is the translational velocity of the center of particle and  $\omega(t)$  is the angular velocity component of the particle. The particle center  $\mathbf{Y}_c(t) = (Y_{1c}(t), Y_{2c}(t))$  thus moves according to  $\frac{d\mathbf{Y}_c}{dt} = \mathbf{V}_c(t)$ . Since the particle center velocity  $\mathbf{V}_c(t)$  and the angular velocity component  $\omega(t)$  are also unknown, the system of equations must be closed by the force-free (2.6) and torque-free (2.7) conditions for a rigid body motion. The torque-free condition is derived in detail in Appendix A.

Like the pressure in incompressible flow, the elastic tension  $\sigma$  and the particle surface force  $\mathbf{F}$  in the present IB formulation are not known a priori, and they must be determined as parts of the solution. In fact, the tension and the particle surface force play the role of Lagrange multipliers in enforcing the local inextensible constraint (2.3) along the interface and the no-slip boundary condition (2.5) along the particle surface, respectively. So the major difficulty of solving the above interfacial problem enclosing a solid particle is that one needs to find those solution variables simultaneously. In this paper, we discretize (2.1)–(2.7) directly and use a fractional step method to solve the resultant linear system of equations. The detailed numerical algorithm will be given in the next section.

In the IB formulation, the force spreading operator and the velocity interpolating operator are self-adjoint in both continuous and discrete senses [16]. Here, we would like to show that the spreading operator acting on the function  $\sigma$  and the surface divergence operator of the velocity are skew-adjoint with each other. To proceed, let us define the spreading operator  $S$  of  $\sigma$  and the surface divergence operator  $\nabla_s$  of  $\mathbf{U}$  as follows:

$$(2.8) \quad S(\sigma) = \int_{\Gamma} \frac{\partial}{\partial s} (\sigma \boldsymbol{\tau}) \delta(\mathbf{x} - \mathbf{X}(s)) \, ds,$$

$$(2.9) \quad \nabla_s \cdot \mathbf{U} = \frac{\partial \mathbf{U}}{\partial s} \cdot \frac{\boldsymbol{\tau}}{\left| \frac{\partial \mathbf{X}}{\partial s} \right|} = \frac{\partial}{\partial s} \left( \int_{\Omega} \mathbf{u}(\mathbf{x}) \delta(\mathbf{x} - \mathbf{X}(s)) \, d\mathbf{x} \right) \cdot \frac{\boldsymbol{\tau}}{\left| \frac{\partial \mathbf{X}}{\partial s} \right|}.$$

We also define the inner product of functions on  $\Omega$  and  $\Gamma$  in the following:

$$(2.10) \quad \langle \mathbf{u}, \mathbf{v} \rangle_\Omega = \int_\Omega \mathbf{u}(\mathbf{x}) \cdot \mathbf{v}(\mathbf{x}) \, d\mathbf{x}, \quad \langle f, g \rangle_\Gamma = \int_\Gamma f(l) g(l) \, dl,$$

where  $l$  in (2.10) is the arc-length parameter. Then we have

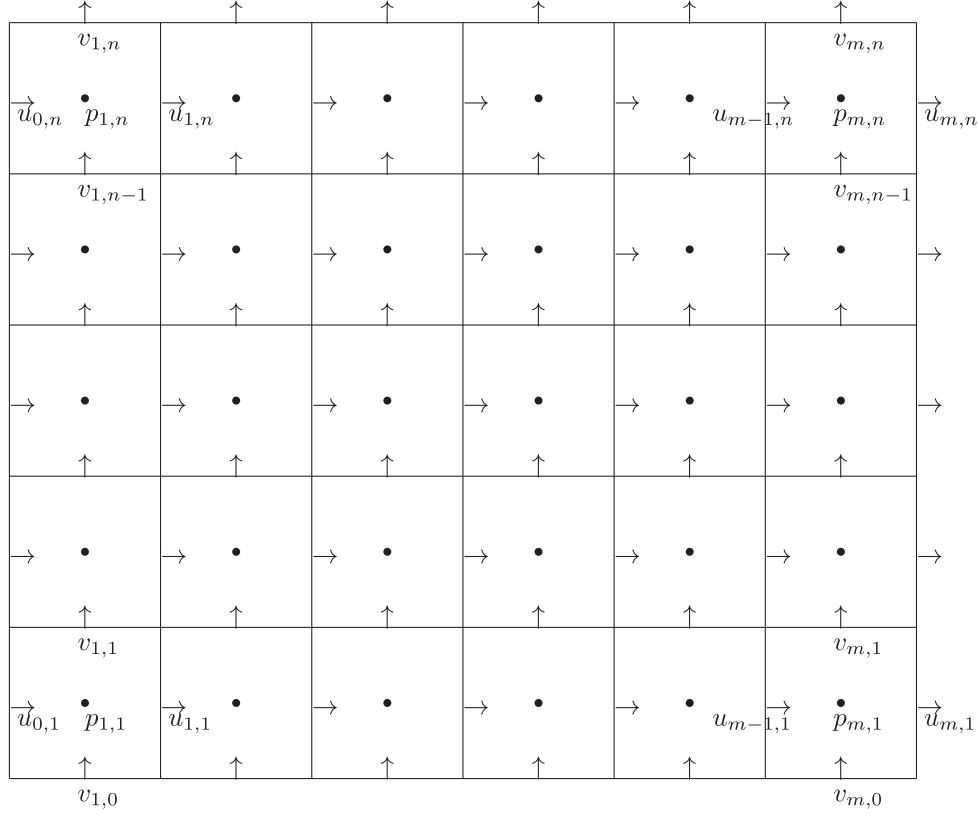
$$(2.11) \quad \begin{aligned} \langle S(\sigma), \mathbf{u} \rangle_\Omega &= \int_\Omega \left( \int_\Gamma \frac{\partial}{\partial s} (\sigma \boldsymbol{\tau}) \delta(\mathbf{x} - \mathbf{X}(s)) \, ds \right) \cdot \mathbf{u}(\mathbf{x}) \, d\mathbf{x} \\ &= \int_\Gamma \frac{\partial}{\partial s} (\sigma \boldsymbol{\tau}) \cdot \left( \int_\Omega \mathbf{u}(\mathbf{x}) \delta(\mathbf{x} - \mathbf{X}(s)) \, d\mathbf{x} \right) \, ds \\ &= - \int_\Gamma \sigma \left( \boldsymbol{\tau} \cdot \frac{\partial \mathbf{U}}{\partial s} \right) \, ds \\ &\quad \text{(integration by parts and the closed interface)} \\ &= \int_\Gamma \sigma \left( - \frac{\partial \mathbf{U}}{\partial s} \cdot \frac{\boldsymbol{\tau}}{|\frac{\partial \mathbf{X}}{\partial s}|} \right) \left| \frac{\partial \mathbf{X}}{\partial s} \right| \, ds \\ &= \langle \sigma, -\nabla_s \cdot \mathbf{U} \rangle_\Gamma = \langle \sigma, S^*(\mathbf{U}) \rangle_\Gamma. \end{aligned}$$

It follows that the spreading operator and the surface divergence operator are skew-adjoint.

The reason for showing the skew-adjointness of those two operators is twofold. First, since the surface divergence of the velocity is zero, the above derivation leads to  $\langle S(\sigma), \mathbf{u} \rangle_\Omega = 0$ . That is, the present elastic tension does not do work to the fluid, which is not surprising since it is merely the Lagrange multiplier for the inextensible constraint. However, if we add bending force along the interface, such as the one in vesicle problems [25, 7], then the bending force does do work to the fluid. Second, the skew-adjointness is also satisfied in the discrete sense (see the next section) so that the resultant matrix is symmetric.

**3. Numerical discretization.** We now are ready to discretize (2.1)–(2.7) by the IB method. For simplicity, we assume that the computational domain  $\Omega = [a, b] \times [c, d]$  is a rectangular domain and that the fluid variables are defined on the staggered marker-and-cell (MAC) grid [4]. That is, as shown in Figure 3.1, the pressure is defined on the grid points labelled as  $\mathbf{x} = (x_i, y_j) = (a + (i - 1/2)\Delta x, c + (j - 1/2)\Delta y)$ ,  $i = 1, 2, \dots, m$  and  $j = 1, 2, \dots, n$ , while the velocity components  $u$  and  $v$  are defined at  $(x_{i-1/2}, y_j) = (a + (i - 1)\Delta x, c + (j - 1/2)\Delta y)$  and  $(x_i, y_{j-1/2}) = (a + (i - 1/2)\Delta x, c + (j - 1)\Delta y)$ , respectively. Here, we assume that a uniform mesh width  $h = \Delta x = \Delta y$  is used, although that is not necessary. For the immersed inextensible interface  $\mathbf{X}$ , we use a collection of discrete points  $s_k = k\Delta s$ ,  $k = 0, 1, \dots, M$ , with the interface mesh width  $\Delta s$  so the Lagrangian markers of the interface are represented by  $\mathbf{X}_k = \mathbf{X}(s_k)$ . Similarly, we use a collection of discrete points  $\alpha_k = k\Delta\alpha$ ,  $k = 0, 1, \dots, M_p$ , so that the particle surface points are represented by  $\mathbf{Y}_k = \mathbf{Y}(\alpha_k)$ . Both  $\Delta s$  and  $\Delta\alpha$  are roughly chosen as a half of fluid mesh  $h$ . Both the interface and the particle surface are closed so that we have  $\mathbf{X}_0 = \mathbf{X}_M$  and  $\mathbf{Y}_0 = \mathbf{Y}_{M_p}$ . The elastic tension is defined at the ‘‘half-integer’’ points given by  $s_{k-1/2} = (k - 1/2)\Delta s$ , so we denote it by  $\sigma_{k-1/2}$ . Without loss of generality, for any function defined on the interface  $\psi(s)$ , we approximate the partial derivative  $\frac{\partial \psi}{\partial s}$  by the centered difference scheme as

$$(3.1) \quad D_s \psi = \frac{\psi(s + \Delta s/2) - \psi(s - \Delta s/2)}{\Delta s}.$$

FIG. 3.1. The computational domain  $\Omega$  with staggered grid.

Thus, the interface stretching factor and the unit tangent can be approximated by  $|D_s \mathbf{X}|$  and  $\boldsymbol{\tau} = D_s \mathbf{X} / |D_s \mathbf{X}|$ , which in turn are also defined at the half-integer points. We denote them by  $|D_s \mathbf{X}|_{k-1/2}$  and  $\boldsymbol{\tau}_{k-1/2}$ , respectively.

Let  $\Delta t$  be the time step size, and the superscript of the variables denote the time step index. At the beginning of each time step  $l$ , the interface configuration  $\mathbf{X}_k^l$ , the particle surface  $\mathbf{Y}_k^l = (Y_{1k}^l, Y_{2k}^l)$ , and its center  $\mathbf{Y}_c^l = (Y_{1c}^l, Y_{2c}^l)$  are all given. Despite the fact that the problem is nonlinear, here we propose a linearly semi-implicit scheme for (2.1)–(2.7). The time step can be advanced as follows:

(3.2)

$$-\nabla_h p^{l+1} + \Delta_h \mathbf{u}^{l+1} + \sum_{k=1}^M D_s (\sigma^{l+1} \boldsymbol{\tau}^l)_k \delta_h(\mathbf{x} - \mathbf{X}_k^l) \Delta s + \sum_{k=1}^{M_p} \mathbf{F}_k^{l+1} \delta_h(\mathbf{x} - \mathbf{Y}_k^l) \Delta \alpha = 0,$$

(3.3)

$$\nabla_h \cdot \mathbf{u}^{l+1} = 0,$$

(3.4)

$$\nabla_{s_h} \cdot \mathbf{U}_k^{l+1} = \frac{\mathbf{U}_k^{l+1} - \mathbf{U}_{k-1}^{l+1}}{\Delta s} \cdot \frac{\boldsymbol{\tau}_{k-1/2}^l}{|D_s \mathbf{X}^l|_{k-1/2}} = 0 \quad \text{for } k = 1, 2, \dots, M,$$

(3.5)

$$\mathbf{U}_k^{l+1} = \sum_{\mathbf{x}} \mathbf{u}(\mathbf{x})^{l+1} \delta_h(\mathbf{x} - \mathbf{X}_k^l) h^2 \quad \text{for } k = 1, 2, \dots, M,$$

$$\begin{aligned}
\mathbf{V}_k^{l+1} &= \sum_{\mathbf{x}} \mathbf{u}(\mathbf{x})^{l+1} \delta_h(\mathbf{x} - \mathbf{Y}_k^l) h^2 \\
(3.6) \quad &= \mathbf{V}_c^{l+1} + \omega^{l+1} \begin{bmatrix} -(Y_{2k}^l - Y_{2c}^l) \\ Y_{1k}^l - Y_{1c}^l \end{bmatrix} \quad \text{for } k = 1, 2, \dots, M_p,
\end{aligned}$$

$$(3.7) \quad \sum_{k=1}^{M_p} \mathbf{F}_k^{l+1} \Delta \alpha = 0,$$

$$(3.8) \quad \sum_{k=1}^{M_p} (F_{1k}^{l+1} (Y_{2k}^l - Y_{2c}^l) - F_{2k}^{l+1} (Y_{1k}^l - Y_{1c}^l)) \Delta \alpha = 0,$$

where the spatial operators  $\nabla_h$ ,  $\Delta_h$ , and  $\nabla_{s_h} \cdot$  are the standard second-order centered difference approximations to the gradient, Laplacian, and surface divergence. Here,  $\delta_h$  is a smoother version of discrete delta function developed in [27] as  $\delta_h(\mathbf{x}) = \frac{1}{h^2} \phi(\frac{x}{h}) \phi(\frac{y}{h})$ , with

$$\phi(r) = \begin{cases} \frac{3}{8} + \frac{\pi}{32} - \frac{r^2}{4}, & |r| < 0.5, \\ \frac{1}{4} + \frac{1-|r|}{8} \sqrt{-2 + 8|r| - 4r^2} - \frac{1}{8} \sin^{-1}(\sqrt{2}(|r| - 1)), & 0.5 \leq |r| \leq 1.5, \\ \frac{17}{16} - \frac{\pi}{64} - \frac{3|r|}{4} + \frac{r^2}{8} + \frac{|r|-2}{16} \sqrt{-14 + 16|r| - 4r^2} \\ + \frac{1}{16} \sin^{-1}(\sqrt{2}(|r| - 2)), & 1.5 \leq |r| \leq 2.5, \\ 0, & 2.5 \leq |r|. \end{cases}$$

One should notice that this discrete delta function has one grid support wider than the one often used in the community. The advantage of using the above smoothing delta function is that it reduces oscillations of the elastic tension caused by the present IB method. The computation for the elastic tension cause oscillations in other literature [28, 7, 11].

Once we obtain the new velocity field  $\mathbf{u}^{l+1}$  on the fluid grid, we can interpolate the new velocity to the marker points by (3.5) and move the Lagrangian markers to new positions. That is,

$$(3.9) \quad \mathbf{X}_k^{l+1} = \mathbf{X}_k^l + \Delta t \mathbf{U}_k^{l+1}.$$

Therefore, we have

$$\frac{\mathbf{X}_k^{l+1} - \mathbf{X}_{k-1}^{l+1}}{\Delta s} = \frac{\mathbf{X}_k^l - \mathbf{X}_{k-1}^l}{\Delta s} + \Delta t \frac{\mathbf{U}_k^{l+1} - \mathbf{U}_{k-1}^{l+1}}{\Delta s}.$$

By multiplying the above equation by itself and using the zero discrete surface divergence (3.4), we obtain the equality

$$\left| \frac{\mathbf{X}_k^{l+1} - \mathbf{X}_{k-1}^{l+1}}{\Delta s} \right|^2 = \left| \frac{\mathbf{X}_k^l - \mathbf{X}_{k-1}^l}{\Delta s} \right|^2 + (\Delta t)^2 \left| \frac{\mathbf{U}_k^{l+1} - \mathbf{U}_{k-1}^{l+1}}{\Delta s} \right|^2,$$

which leads to

$$(3.10) \quad |D_s \mathbf{X}^{l+1}|_{k-1/2}^2 = |D_s \mathbf{X}^l|_{k-1/2}^2 + (\Delta t)^2 |D_s \mathbf{U}^{l+1}|_{k-1/2}^2.$$

Thus, we conclude that the pointwise error for the local stretching factor is first-order accurate, which is comparable to the accuracy of the IB method.

For the solid particle motion, the particle center velocity  $\mathbf{V}_c$  and the angular velocity component  $\omega$  will be solved as parts of the solution. Instead of first using the interpolation formula to find the new velocity and then updating the particle surface points, we simply adopt the idea of rigid body motion to determine the particle surface position. That is, we compute the new particle center and the rotational angle by

$$(3.11) \quad \mathbf{Y}_c^{l+1} = \mathbf{Y}_c^l + \Delta t \mathbf{V}_c^{l+1}, \quad \theta^{l+1} = \theta^l + \Delta t \omega^{l+1},$$

and then use them to find the new particle surface position as

$$(3.12) \quad \mathbf{Y}_k^{l+1} = \mathbf{Y}_c^{l+1} + \begin{bmatrix} \cos \theta^{l+1} & -\sin \theta^{l+1} \\ \sin \theta^{l+1} & \cos \theta^{l+1} \end{bmatrix} \mathbf{Y}_k^0.$$

#### 4. Implementation details.

**4.1. Discrete skew-adjoint operators.** In this subsection, we show that the spreading operator  $S$  acting on the elastic tension and the surface divergence operator  $\nabla_s$  acting on the velocity are also skew-adjoint in the discrete sense. That is, we shall prove the numerical identity for (2.11). To proceed, we first define the corresponding discrete inner product on the fluid grid  $\Omega_h$  and the interfacial grid  $\Gamma_h$  as

$$(4.1) \quad \langle \mathbf{u}, \mathbf{v} \rangle_{\Omega_h} = \sum_{\mathbf{x}} \mathbf{u}(\mathbf{x}) \cdot \mathbf{v}(\mathbf{x}) h^2, \quad \langle \phi, \psi \rangle_{\Gamma_h} = \sum_{k=1}^M \phi_{k-1/2} \psi_{k-1/2} |D_s \mathbf{X}|_{k-1/2} \Delta s,$$

where the second summation is nothing but the midpoint rule for the second integral of (2.10). We also define the discrete spreading operator  $S_h$  acting on the discrete elastic tension  $\sigma_h$  as

$$(4.2) \quad S_h(\sigma_h) = \sum_{k=1}^M D_s(\sigma \boldsymbol{\tau})_k \delta_h(\mathbf{x} - \mathbf{X}_k) \Delta s.$$

Then we have

$$\begin{aligned} \langle S_h(\sigma_h), \mathbf{u} \rangle_{\Omega_h} &= \sum_{\mathbf{x}} \left( \sum_{k=1}^M D_s(\sigma \boldsymbol{\tau})_k \delta_h(\mathbf{x} - \mathbf{X}_k) \Delta s \right) \cdot \mathbf{u}(\mathbf{x}) h^2 \\ &= \sum_{k=1}^M D_s(\sigma \boldsymbol{\tau})_k \cdot \left( \sum_{\mathbf{x}} \mathbf{u}(\mathbf{x}) \delta_h(\mathbf{x} - \mathbf{X}_k) h^2 \right) \Delta s = \sum_{k=1}^M D_s(\sigma \boldsymbol{\tau})_k \cdot \mathbf{U}_k \Delta s \\ &= \sum_{k=1}^M \frac{\sigma_{k+1/2} \boldsymbol{\tau}_{k+1/2} - \sigma_{k-1/2} \boldsymbol{\tau}_{k-1/2}}{\Delta s} \cdot \mathbf{U}_k \Delta s \\ &= - \sum_{k=1}^M \sigma_{k-1/2} \left( \frac{\mathbf{U}_k - \mathbf{U}_{k-1}}{\Delta s} \right) \cdot \boldsymbol{\tau}_{k-1/2} \Delta s \quad (\text{summation by parts}) \\ &= \langle \sigma_h, -\nabla_{s_h} \cdot \mathbf{U} \rangle_{\Gamma_h} = \langle \sigma_h, S_h^*(\mathbf{U}) \rangle_{\Gamma_h}. \end{aligned}$$

Note that this discrete skew-adjoint property is crucial to our IB formulation for solving (3.2)–(3.8). Due to the fact that discrete surface divergence of the velocity is

zero in (3.4), we can rescale this constraint to make the resultant matrix obtained by (3.4) be the transpose of the matrix obtained by the discrete spreading operator of the tension. One can also verify this symmetric property by expressing those terms explicitly, which is given in Appendix B.

**4.2. Existence of a solution.** By using the staggered grid to discretize the fluid variables, the matrix obtained by the discrete divergence of the fluid velocity can be written as the transpose of the discrete gradient of the pressure. As derived before, the matrix obtained by the discrete surface divergence of the velocity can be written as the transpose of the matrix obtained by the discrete spreading operator of the tension. Similarly, the matrix obtained by the discrete spreading operator of the force arising from the particle solid boundary can be written as the transpose of the matrix obtained by the discrete interpolating operator of velocity. Thus, the linear system for (3.2)–(3.8) is symmetric and can be written as

$$(4.3) \quad \begin{bmatrix} L & G & S & E & 0 \\ G^T & 0 & 0 & 0 & 0 \\ S^T & 0 & 0 & 0 & 0 \\ E^T & 0 & 0 & 0 & R \\ 0 & 0 & 0 & R^T & 0 \end{bmatrix} \begin{bmatrix} \mathbf{u} \\ p \\ \sigma \\ \mathbf{F} \\ \Theta \end{bmatrix} = \begin{bmatrix} bc_1 \\ bc_2 \\ 0 \\ 0 \\ 0 \end{bmatrix},$$

where the submatrix  $L$ ,  $G$ ,  $S$ ,  $E$ , and  $R$  represents the discrete Laplacian  $\Delta_h$ , discrete gradient  $-\nabla_h$ , the discrete spreading operator  $S_h$  on tension, the discrete spreading operator  $E_h$  on the surface force, and the discrete rigid body motion equation. The submatrix sizes of  $L$ ,  $G$ ,  $S$ ,  $E$ , and  $R$  are  $((m-1)n+m(n-1)) \times ((m-1)n+m(n-1))$ ,  $((m-1)n+m(n-1)) \times (mn)$ ,  $(m-1)n+m(n-1) \times M$ ,  $(m-1)n+m(n-1) \times 2M_p$ , and  $2M_p \times 3$ , respectively. The unknown  $\Theta = [V_{1c}, V_{2c}, \omega]^T$ ; the right-hand-side vector  $[bc_1, bc_2, 0, 0, 0]^T$  of (4.3) consists only of the velocity boundary conditions, since the pressure does not need the boundary condition in the present grid arrangement. The detailed entities of the submatrices  $S$  and  $R$  can be found in Appendices A and B.

Let us discuss the existence of the solution for the linear system (4.3). For clarity, we denote the matrix in (4.3) by  $A$ . As known, without the effects of the inextensible interface and the solid particle, the problem becomes pure Stokes flow, and the linear system is

$$(4.4) \quad \begin{bmatrix} L & G \\ G^T & 0 \end{bmatrix} \begin{bmatrix} \mathbf{u} \\ p \end{bmatrix} = \begin{bmatrix} bc_1 \\ bc_2 \end{bmatrix}.$$

Let us denote the matrix in (4.4) by  $\tilde{A}$ . It is wellknown that the nullity of  $\tilde{A}$  equals 1 since the pressure is unique up to a constant, and the existence of a solution can be verified by using the discrete incompressible constraint (3.3). To be precise, since the rank of deficiency of  $\tilde{A}$  is 1, based on the algebraic structure of the submatrix  $G$ , the kernel of  $\tilde{A}$  is

$$(4.5) \quad \ker(\tilde{A}) = \text{span}\left\{ \left[ \underbrace{0 \cdots 0}_{(m-1)n+m(n-1)} \quad \underbrace{1 \cdots 1}_{mn} \right]^T \right\}.$$

And for any vector  $z \in \ker(\tilde{A}^T) = \ker(\tilde{A})$ , we have

$$\begin{aligned}
z^T \begin{bmatrix} bc_1 \\ bc_2 \end{bmatrix} &= \sum_{k=1}^{mn} (bc_2)_k = \sum_{j=1}^n \frac{u_{0,j}}{h} - \sum_{j=1}^n \frac{u_{m,j}}{h} + \sum_{i=1}^m \frac{v_{i,0}}{h} - \sum_{i=1}^m \frac{v_{i,n}}{h} \\
&= - \left( - \sum_{j=1}^n u_{0,j} h + \sum_{j=1}^n u_{m,j} h - \sum_{i=1}^m v_{i,0} h + \sum_{i=1}^m v_{i,n} h \right) h^{-2} \\
&= \left( \sum_{i=1}^m \sum_{j=1}^n \left( \frac{u_{i,j} - u_{i-1,j}}{h} + \frac{v_{i,j} - v_{i,j-1}}{h} \right) h^2 \right) h^{-2} \\
(4.6) \quad &= 0 \quad (\text{by the discrete incompressibility (3.3)}),
\end{aligned}$$

which shows the compatibility condition for the existence of a solution.

If we add the effects of the interface and the solid particle, then the matrix  $\tilde{A}$  is augmented by additional submatrices to become  $A$  as in (4.3). Since the matrices  $S$  and  $E$  come from the discrete spreading operator, the entries of  $S$  and  $E$  depend on the positions of moving Lagrangian markers. It is unlikely to show rigorously that the nullity of  $A$  is exactly equal to 1; however, we have confirmed the above statement to be true in our numerical experiments. So the apparent kernel can be

$$(4.7) \quad \ker(A) = \text{span}\left\{ \begin{bmatrix} \underbrace{0 \cdots 0}_{(m-1)n+m(n-1)} & \underbrace{1 \cdots 1}_{mn} & \underbrace{0 \cdots 0}_M & \underbrace{0 \cdots 0}_{2M_p} & \underbrace{0, 0, 0}_3 \end{bmatrix}^T \right\},$$

and the existence of a solution for the linear system (4.3) follows the equality of (4.6) immediately.

**4.3. Fractional step method.** In this subsection, we apply the idea of the fractional step method developed by Taira and Colonius [24] to solve the resultant linear system of equations (4.3). In [24], the authors applied the IB method to simulate the incompressible flow over solid bodies with prescribed body surface velocity. Unlike the previous feedback forcing approaches in [5, 19, 12], they introduced the boundary force as another Lagrange multiplier to enforce the no-slip condition for the velocity at the immersed boundary. From this point of view, the present approach shares the spirit of [24] by introducing the elastic tension as a new Lagrange multiplier to enforce the surface divergence-free constraint (3.4) along the interface. Thus, it is natural to group all Lagrange multipliers into a new column vector  $q = [p, \sigma, \mathbf{F}, \Theta]^T$  and combine the submatrices  $G$ ,  $S$ , and  $E$  as  $Q = [G, S, E, 0]$ , so the linear system (4.3) becomes

$$(4.8) \quad \begin{bmatrix} L & Q \\ Q^T & D \end{bmatrix} \begin{bmatrix} \mathbf{u} \\ q \end{bmatrix} = \begin{bmatrix} bc_1 \\ \tilde{b} \end{bmatrix}, \quad \text{where } D = \begin{bmatrix} 0 & 0 & 0 & 0 \\ 0 & 0 & 0 & 0 \\ 0 & 0 & 0 & R \\ 0 & 0 & R^T & 0 \end{bmatrix} \quad \text{and } \tilde{b} = \begin{bmatrix} bc_2 \\ 0 \\ 0 \\ 0 \end{bmatrix}.$$

As in [24], we perform a block LU decomposition to the above equation to obtain

$$(4.9) \quad \begin{bmatrix} L & 0 \\ Q^T & -Q^T L^{-1} Q + D \end{bmatrix} \begin{bmatrix} I & L^{-1} Q \\ 0 & I \end{bmatrix} \begin{bmatrix} \mathbf{u} \\ q \end{bmatrix} = \begin{bmatrix} bc_1 \\ \tilde{b} \end{bmatrix}.$$

Note that the above decomposition is possible ( $L^{-1}$  exists) since the matrix  $L$  arising from the discrete Laplacian operator is symmetric and negative definite. One can further split the above matrix equation into the following steps by introducing an intermediate velocity  $\mathbf{u}^*$ :

$$(4.10) \quad L\mathbf{u}^* = bc_1,$$

$$(4.11) \quad (-Q^T L^{-1} Q + D)q = \tilde{b} - Q^T \mathbf{u}^*,$$

$$(4.12) \quad \mathbf{u} = \mathbf{u}^* - L^{-1} Qq.$$

Now we are ready to describe the detailed numerical implementation for solving (4.10)–(4.12). It is common practice to avoid the direct computation of the inverse of the matrix  $L$  since it is too expensive. In [24], a second-order approximation for  $L^{-1}$  based on Taylor expansion is implemented for solving equations similar to our (4.11)–(4.12), and the conjugate gradient method is applied to solve those equations iteratively. However, this leads to another time step constraint related to the viscosity and the eigenvalues of the discrete Laplacian. In this paper, since we are working on the Stokes flow rather than the Navier–Stokes, we are unable to approximate  $L^{-1}$  using Taylor’s expansion. Although we do not approximate the  $L^{-1}$  directly, we still can solve (4.10)–(4.12) efficiently thanks to the fast Poisson solver developed in public software package FISHPACK [1]. (The present matrix  $L$  is nothing but the discrete Laplacian operator.) The detailed steps for solving (4.10)–(4.12) are as follows:

*Step 1.* Solve (4.10) by two fast Poisson solvers to obtain intermediate velocity field  $\mathbf{u}^*$ .

*Step 2.* Solve (4.11) by the GMRES method. In each iteration, a matrix-vector product  $(-Q^T L^{-1} Q)\varphi$  is needed; fortunately, this can be obtained by letting  $z = L^{-1} Q\varphi$  and solving  $Lz = Q\varphi$ . Once it is done, we multiply  $z$  by  $-Q^T$  to obtain the product needed. Again, the time-consuming cost in each iteration is one fast Poisson solver.

*Step 3.* Find the velocity field  $\mathbf{u}$  from (4.12). Since  $q$  is solved via Step 2, by solving  $L\mathbf{w} = Qq$ , we then obtain  $\mathbf{u} = \mathbf{u}^* - \mathbf{w}$ . Again, this involves applying two fast Poisson solvers.

Therefore, the overall cost in Steps 1–3 for our present numerical algorithm can be counted in terms of the number of fast Poisson solvers applied. In the next section, we shall show the numbers of fast Poisson solvers used in the Stokes flow for different grid resolutions.

**5. Numerical results.** In this section, we perform a series of numerical tests for the present scheme. Throughout this section, the computational domain is chosen as  $\Omega = [-1, 1] \times [-1, 1]$ . All numerical runs were carried out on a PC with 4G of RAM using double precision arithmetics.

**5.1. Convergence and efficiency tests for the Stokes solver.** In this subsection, we perform the convergence test and evaluate the efficiency for the present Stokes solver. The numerical algorithm for solving this problem is exactly same as Steps 1–3 described in the previous section but in a simpler manner; that is,  $Q = G$  and  $q = p$ . Other efficient Stokes solvers can be found in [23, 2, 18] and the references therein.

Here, we use the following test example so that we can easily compute the errors between the exact and numerical solutions:

$$u_e(x, y) = \sin x \cos y, \quad v_e(x, y) = -\cos x \sin y, \quad \text{and} \quad p_e(x, y) = e^x \sin y.$$

TABLE 5.1  
*Numerical accuracy for the Stokes solver.*

$m = n$	32	64	128	256	512
$\ u_e - u_h\ _\infty$	1.578e-4	4.481e-5	1.206e-5	3.153e-6	8.120e-7
Rate	-	1.82	1.89	1.94	1.96
$\ v_e - v_h\ _\infty$	1.578e-4	4.481e-5	1.206e-5	3.153e-6	8.120e-7
Rate	-	1.82	1.89	1.94	1.96
$\ p_e - p_h\ _\infty$	9.615e-4	4.286e-4	2.052e-4	1.005e-4	4.970e-5
Rate	-	1.17	1.06	1.03	1.02

TABLE 5.2  
*The cost in CPU time and iterations.*

$m = n$	32	64	128	256	512
Iterations	12	14	15	16	18
CPU time(sec)	0.02	0.05	0.20	0.93	4.97

Note that the above solution does not satisfy the pure Stokes equations, so we need to add some external force field (can be easily computed) into the equations. However, it does not change the method or algorithm since the extra force term appears on the right-hand side of equations. Along the boundary of computational domain, the Dirichlet boundary conditions for the velocity are provided, while no pressure boundary condition is needed in our setting.

It is worth mentioning that the pressure is unique up to a constant in Stokes equations. Rather than pinning a certain value to a particular discrete pressure as in [24], uniqueness can be guaranteed by setting up a constraint for the discrete pressure as

$$(5.1) \quad \sum_{i,j} p_{i,j} h^2 = \int_{\Omega} p_e(\mathbf{x}) d\mathbf{x}.$$

So our initial guess  $p_{ij}^0$  in the GMRES iteration can be chosen as  $p_{ij}^0 = \int_{\Omega} p_e(\mathbf{x}) d\mathbf{x} / |\Omega|$ . In those tests, the tolerance of the residual is chosen as  $10^{-8}$ .

Table 5.1 shows the maximum errors between the exact and numerical solutions for different grid resolutions. One can see that the velocity field has clear second-order accuracy, while the pressure has first-order accuracy. Table 5.2 shows the efficiency of the present Stokes solver. One can see that the number of iterations increases slightly even we double the grid size, and the CPU time for a  $512 \times 512$  grid is just a few seconds.

**5.2. Convergence test for the Stokes flow with an inextensible interface enclosing a solid particle.** In this subsection, we perform a convergence study for the present numerical algorithm to the Stokes flow with an inextensible interface enclosing a solid particle. Here, we put an inextensible interface  $\Gamma$  and particle  $P$  with initial configuration  $\mathbf{X}(s) = (0.25 \cos(s), 0.5 \sin(s))$  and  $\mathbf{Y}(s) = (0.1 \cos(s), 0.1 \sin(s))$  under a shear flow  $(u, v) = (\chi y, 0)$  in a fluid domain  $\Omega$ . The dimensionless shear rate  $\chi$  is chosen to be  $\chi = 1$ . We also choose the different grid size as  $m = n = 32, 64, 128, 256, 512$  in which the corresponding mesh width is  $h = 2/m$ . We also set the Lagrangian mesh widths to be  $\Delta s \approx h/2$  and  $\Delta \alpha \approx h/2$ , and the time step size to  $\Delta t = h/4$ .

Since the analytical solution is not available in this test, we choose the result obtained from the finest mesh  $m = n = 512$  as our reference solution and compute the

TABLE 5.3

The mesh refinement results for the perimeter of the interface  $L_h$ , the interface configuration  $\mathbf{X}_h$ , and the velocity  $u_h$  and  $v_h$ .

	$m = 32$	$m = 64$	rate	$m = 128$	rate	$m = 256$	rate
$ L_h - L_0 /L_0$	3.511e-2	2.089e-2	0.75	1.220e-2	0.78	6.749e-3	0.85
$\ \mathbf{X}_h - \mathbf{X}_{\text{ref}}\ _\infty$	3.413e-3	1.079e-3	1.66	4.438e-4	1.28	1.622e-4	1.45
$\ u_h - u_{\text{ref}}\ _\infty$	6.552e-2	2.592e-2	1.34	1.053e-2	1.30	4.047e-3	1.38
$\ v_h - v_{\text{ref}}\ _\infty$	1.133e-1	3.660e-2	1.63	1.554e-2	1.24	4.968e-3	1.64

maximum error between the reference and the numerical solutions. All the numerical solutions are computed up to time  $T = 0.0625$ . Since the interface is inextensible, the perimeter of the interface should remain a constant theoretically as time evolves. Let  $L_0$  and  $L_h$  be the perimeters of the interface at the initial time and final time  $T = 0.0625$ , respectively. The relative error of the perimeter is defined as  $|L_h - L_0|/L_0$ . Table 5.3 shows the relative errors of the perimeter, the maximum errors of the interface configuration, and the maximum errors for the fluid velocity field. Note that the fluid variables are defined at the staggered grid, so when we refine the mesh, the numerical solutions will not coincide with the same grid locations. In these runs, we simply use a linear interpolation to compute the solutions at the desired locations. Due to the fact that the IB formulation has the singular forcing term in the equations, regularizing the singular term by smoothing the discrete delta function causes the method to be first-order accurate. As shown in [3], even though the calculated pressure has  $O(1)$  error near the interface, its gradient has the same discretization error as the singular delta force term near the interface. Thus, the overall accuracy of the velocity field in the IB method is first-order accurate in the  $L_\infty$  norm. The numerical results shown in Table 5.3 are consistent with what we expect from theory.

**5.3. Tank-treading to tumbling motion under shear flow.** Unlike the previous subsection where we focus on the numerical convergence test for our present scheme, here we consider the physical transient deformation of an inextensible interface with or without an enclosing rigid particle in a simple shear flow. As mentioned before, the motivation of this test is to simulate the compound vesicle dynamics, which have a lot of applications in bio-fluid problems [26].

In the present numerical experiments, we choose the residual tolerance for GMRES as  $10^{-4}$ , which is larger than the pure Stokes flow. This is because the elastic tension  $\sigma$  tends to oscillate along the interface, which makes the GMRES method solving (4.11) difficult to converge if the residual tolerance is too small. It will be more appealing if one can find a good preconditioner for solving linear system (4.11) so that GMRES method can converge faster. However, this issue has not yet been resolved.

We first consider the case of an inextensible interface without enclosing a solid particle in a simple shear flow. It is wellknown that the equilibrium dynamics of an inextensible interface or vesicle under a simple shear flow will undergo a tanking-treading motion if the viscosity contrast is under a certain threshold [8]. Here, by tanking-treading motion we mean that the configuration of the interface remains stationary while there is a tangential motion along the interface. As studied in previous literature [28, 9, 10, 25, 7], the motion of this steady interface can be characterized by both the inclination angle  $\theta$  between the long axis of interface and the flow direction, and the

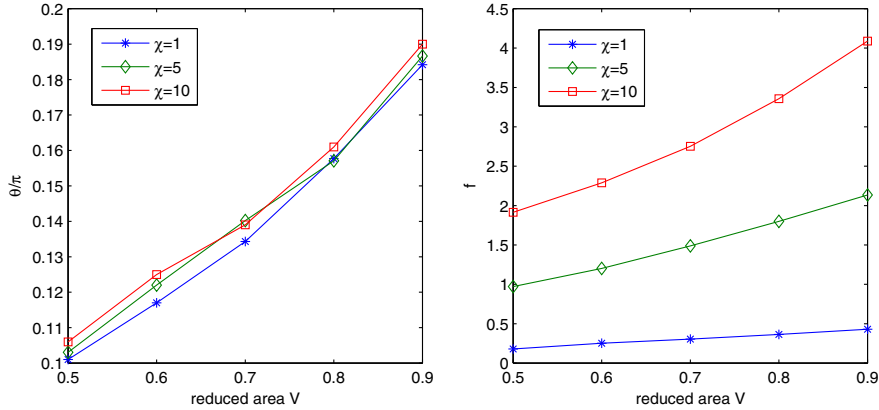


FIG. 5.1. The inclination angles  $\theta/\pi$  (left) and the tank-treading frequency  $f = 2\pi/\int_{\Gamma} \frac{dl}{u_{\tau}} \cdot \boldsymbol{\tau}$  (right) versus reduced areas  $V$  with different dimensionless shear rates for the tank-treading motion of an inextensible interface in a shear flow.

tank-treading frequency  $f = 2\pi/\int_{\Gamma} \frac{dl}{u_{\tau}}$  of the revolution, where  $u_{\tau}$  is the tangential velocity component. The inclination angle has been found to be strongly dependent on the reduced area  $V = \frac{4\pi A_0}{L_0^2}$ , where  $A_0$  is the enclosed area of the interface and  $L_0$  is the total length of interface. (Notice that, by the above definition, a circle has the reduced area  $V = 1$ , while an ellipse with larger aspect ratio has a smaller reduced area.) However, the inclination angle is independent of the dimensionless shear rate  $\chi$ . This behavior is verified in the left panel of Figure 5.1, which shows the steady inclination angle ( $\theta/\pi$ ) versus the reduced area ( $V$ ) with different shear rates  $\chi = 1, 5, 10$ , and it is in a good agreement with previous studies [28, 9, 10, 25, 7]. As the reduced area increases, the inclination angle increases as well. The right panel of Figure 5.1 shows the tank-treading frequency  $f$  versus the reduced area  $V$  for different shear rates. One can see that as the dimensionless shear rate increases, the tangential motion becomes stronger; thus, the frequency becomes larger. Moreover, by fixing the shear rate, if the interface has larger reduced area, then it has larger frequency as well. Again, our numerical results are in good agreement with previous studies in the literature.

Now we consider the case of an inextensible interface enclosing a solid particle (a compound interface) under a shear flow. As shown in [26], the compound interfacial dynamics will have the transition from tank-treading (TT) to tumbling (TB) if the inclusion effect is strong enough. That is, if the filling fraction  $\phi = a^2\pi/A_0$  of the particle ( $a$  is the inclusion particle radius,  $A_0$  is the interface enclosing area) is above some critical threshold, then the interface will start to tumble rather than being stationary. This can be explained as follows. By including a solid particle, the energy dissipation enhances, so the compound interface behaves like an inclusion-free interface that encapsulates a more viscous fluid. The larger the inclusion is, the higher the viscosity will be. Figures 5.2 and 5.3 show the time evolutionary plots for interfacial configurations with different filling fractions,  $\phi = 0.08$  and  $\phi = 0.42$ , respectively. One can indeed see that in the smaller filling fraction case in Figure 5.2, the compound interface has TT motion, while in the larger filling fraction case in Figure 5.3, it has the TB motion.

Meanwhile, in the TT regime, as the filling fraction increases, both the inclination angle and the TT frequency will decrease. Besides, as in the inclusion-free case, the

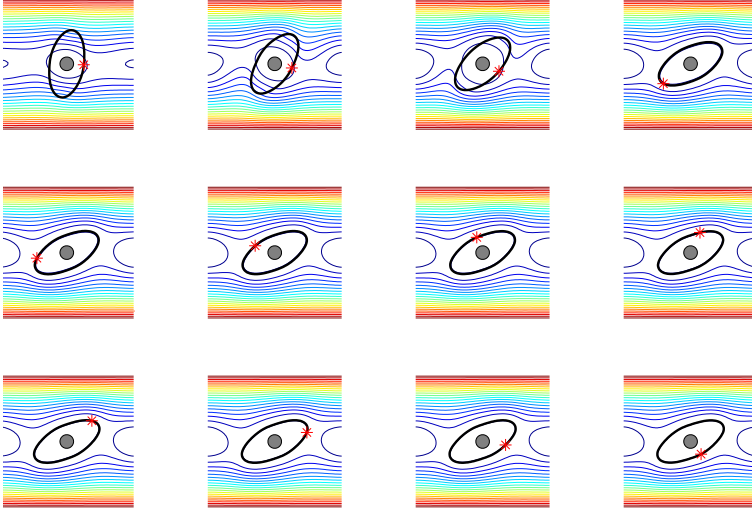


FIG. 5.2. *The motion of an compound interface in a shear flow with initial configuration  $\mathbf{X}(s) = (0.25 \cos(s), 0.5 \sin(s))$  and  $\mathbf{Y}(s) = (0.1 \cos(s), 0.1 \sin(s))$ .  $\phi = 0.08$ .*

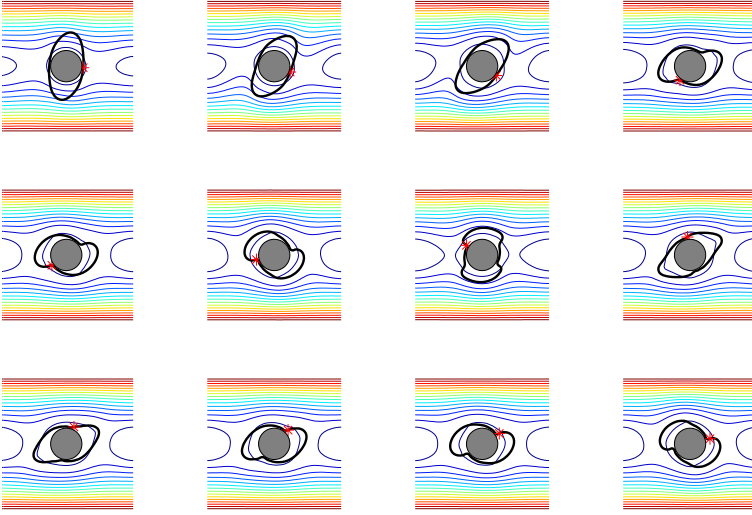


FIG. 5.3. *The motion of an compound interface in a shear flow with initial configuration  $\mathbf{X}(s) = (0.25 \cos(s), 0.5 \sin(s))$  and  $\mathbf{Y}(s) = (0.23 \cos(s), 0.23 \sin(s))$ .  $\phi = 0.42$ .*

compound interface with larger reduced area has larger inclination angle and TT frequency when the filling fraction is small. Both behaviors can be confirmed in Figure 5.4 and are consistent qualitatively with those in [26].

We also investigate the critical value of filling fraction versus the reduced area for the TT motion to TB transition, as in Figure 5.5. Above the critical value, the interface motion will transit from TT to TB. One can easily see that as the reduced area increases, the critical filling fraction increases too. This is exactly the similar behavior as the inclusion-free case in which the critical viscosity contrast increases with the reduced area.

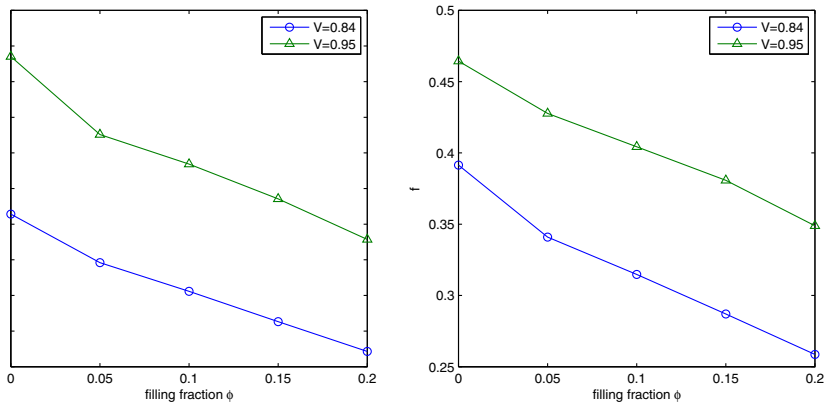


FIG. 5.4. The inclination angles  $\theta/\pi$  (left) and the tank-treading frequency  $f = 2\pi/\int_{\Gamma} \frac{dl}{\mathbf{u} \cdot \boldsymbol{\tau}}$  versus filling fraction  $\phi$  in the tank-treading regime.

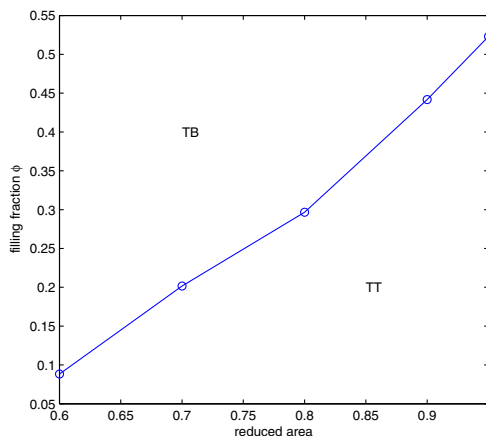


FIG. 5.5. The critical filling fraction for the TT to TB transition versus the reduced area.

**6. Conclusions.** Biological fluid mechanics often require one to study the dynamics of a lipid membrane encapsulating some cellular contents. For instance, a compound vesicle usually consists of a lipid bilayer membrane enclosing a fluid with a suspended particle. Since the bilayer membrane resists area dilation and its thickness is on the order of a nanometer, one can regard the membrane as an inextensible (incompressible) interface. In this paper, we consider the problem of an inextensible interface enclosing a solid particle in Stokes flow. We first write the governing equations in the immersed boundary (IB) framework, in which the interface and solid boundary are treated as force generators in the fluid. In addition to solving for the fluid variables, the present problem involves finding an extra unknown elastic tension such that the surface divergence of the velocity is zero along the interface, and an extra unknown particle surface force such that the velocity satisfies the no-slip boundary condition along the particle surface. We show that the spreading operator of the tension and the surface divergence operator of the velocity are skew-adjoint mathematically. While the interface moves with local fluid velocity, the enclosed particle hereby undergoes a rigid body motion, and the system is closed by the force-free and torque-free conditions along the particle surface.

The governing equations are then discretized by standard centered difference schemes on a staggered grid, and the interactions between the interface and particle and the fluid are discretized using discrete delta function as in the IB method. The discrete spreading operator of the tension and the discrete surface divergence operator of the velocity used in the present scheme preserve the skew-adjoint property numerically. The resultant linear system of equations is therefore symmetric and can be solved by fractional steps so that only fast Poisson solvers are involved. The present method can be extended to Navier–Stokes flow with moderate Reynolds number by treating the nonlinear advection terms explicitly for the time integration. It is also important to mention that, unlike our previous work using the penalty approach [7], we are able to estimate the local error of inextensibility for two successive time steps in the present scheme. In addition, since there are no penalty parameters introduced as in [7], the time step size can be significantly increased.

We study the tank-treading (TT) and tumbling (TB) dynamics for an inextensible interface enclosing a solid particle with different filling fractions under shear flow. We have found that by the increase of the filling fraction, the interface tends to transit from TT to TB. In the TT regime (when the filling fraction is small), the inclination angle and TT frequency will increase as the reduced area increases. Those angle and frequency will decrease as the filling fraction increases. We also have found that the critical filling fraction (from TT to TB) will increase as the reduced area increases, which is qualitatively consistent with the results in [26].

**Appendix A.** In this appendix, we first give a simple derivation for the rigid particle motion equation (2.5) and the torque-free condition (2.7) in twodimensions. These can be derived directly from the following equations in threedimensions,

$$\mathbf{V} = \mathbf{V}_c + \boldsymbol{\omega} \times (\mathbf{Y} - \mathbf{Y}_c), \quad \int_{\partial P} \mathbf{F} \times (\mathbf{Y} - \mathbf{Y}_c) dP = 0,$$

by setting the third component of the vector-valued functions to be zero. For instance, we set  $\mathbf{V} = (V_1, V_2, 0)$ , so the vorticity vector  $\boldsymbol{\omega} = (0, 0, \omega)$ .

The symmetric property of the (3.6)–(3.8) can be seen as follows:

$$\begin{aligned} V_{1k} &= V_{1c} - \omega(Y_{2k} - Y_{2c}), & V_{2k} &= V_{2c} + \omega(Y_{1k} - Y_{1c}), \\ \sum_{K=1}^{M_p} F_{1k} \Delta\alpha &= 0, & \sum_{k=1}^{M_p} F_{2k} \Delta\alpha &= 0, \\ \sum_{k=1}^{M_p} (F_{1k}(Y_{2k} - Y_{2c}) - F_{2k}(Y_{1k} - Y_{1c})) \Delta\alpha &= 0. \end{aligned}$$

We can scale out the coefficient  $\Delta\alpha$  so that the above three equations can be written in the matrix form

$$\begin{bmatrix} 0 & R \\ R^T & 0 \end{bmatrix} \begin{bmatrix} \mathbf{F} \\ \Theta \end{bmatrix}, \quad \text{where } R = \begin{bmatrix} 1 & 0 & -(Y_{21} - Y_{2c}) \\ \vdots & \vdots & \vdots \\ 1 & 0 & -(Y_{2M_p} - Y_{2c}) \\ 0 & 1 & (Y_{11} - Y_{1c}) \\ \vdots & \vdots & \vdots \\ 0 & 1 & (Y_{1M_p} - Y_{1c}) \end{bmatrix} \quad \text{and } \Theta = \begin{bmatrix} V_{1c} \\ V_{2c} \\ \omega \end{bmatrix}.$$

**Appendix B.** In this appendix, we derive that the matrix obtained from the discrete spreading operator  $S_h$  of  $\sigma_h$  and the matrix obtained from discrete surface divergence operator  $\nabla_{s_h}$  of  $\mathbf{U}$  are transpose with each other. To see this, we first rewrite the operator  $S_h(\sigma_h)$  as

$$\begin{aligned}
S_h(\sigma_h) &= \sum_{k=0}^{M-1} D_s(\sigma\boldsymbol{\tau})_k \delta_h(\mathbf{x} - \mathbf{X}_k) \Delta s \\
&= \sum_{k=0}^{M-1} \frac{\sigma_{k+1/2} \boldsymbol{\tau}_{k+1/2} - \sigma_{k-1/2} \boldsymbol{\tau}_{k-1/2}}{\Delta s} \delta_h(\mathbf{x} - \mathbf{X}_k) \Delta s \\
&= \sum_{k=1}^M \sigma_{k-1/2} \boldsymbol{\tau}_{k-1/2} \delta_h(\mathbf{x} - \mathbf{X}_{k-1}) - \sum_{k=1}^M \sigma_{k-1/2} \boldsymbol{\tau}_{k-1/2} \delta_h(\mathbf{x} - \mathbf{X}_k) \\
&\quad - \sigma_{-1/2} \boldsymbol{\tau}_{-1/2} \delta_h(\mathbf{x} - \mathbf{X}_0) + \sigma_{M-1/2} \boldsymbol{\tau}_{M-1/2} \delta_h(\mathbf{x} - \mathbf{X}_M) \\
&= \sum_{k=1}^M (\delta_h(\mathbf{x} - \mathbf{X}_{k-1}) - \delta_h(\mathbf{x} - \mathbf{X}_k)) \boldsymbol{\tau}_{k-1/2} \sigma_{k-1/2}.
\end{aligned}$$

Note that the last two terms are cancelled out due to the periodicity of the interface. Now we can write the discrete operator  $\nabla_{s_h}$  as

$$\begin{aligned}
\nabla_{s_h} \cdot \mathbf{U}_k &= \frac{\mathbf{U}_k - \mathbf{U}_{k-1}}{\Delta s} \cdot \frac{\boldsymbol{\tau}_{k-1/2}}{|D_s \mathbf{X}|_{k-1/2}} \\
&= -\frac{h^2}{\Delta s |D_s \mathbf{X}|_{k-1/2}} \sum_{\mathbf{x}} (\delta_h(\mathbf{x} - \mathbf{X}_{k-1}) - \delta_h(\mathbf{x} - \mathbf{X}_k)) \boldsymbol{\tau}_{k-1/2} \cdot \mathbf{u}_{i,j}.
\end{aligned}$$

Since the discrete surface divergence operator of the velocity is zero, we can scale out the coefficient  $-\frac{h^2}{\Delta s |D_s \mathbf{X}|_{k-1/2}}$  so that the resultant matrices obtained from  $S_h$  and  $\nabla_{s_h} \cdot$  are transpose to each other.

**Acknowledgments.** We thank Xiaofan Li for helping with the formulation of the motion of the solid particle.

#### REFERENCES

- [1] J. ADAMS, P. SWARZTRAUBER, AND R. SWEET, *Fishpack*, a package of Fortran subprograms for the solution of separable elliptic partial differential equations, 1980; see <http://www2.cisl.ucar.edu/resources/legacy/fishpack>.
- [2] J. H. BRAMBLE, J. E. PASCIAK, AND A. T. VASSILEV, *Analysis of the inexact Uzawa algorithm for saddle point problems*, SIAM J. Numer. Anal., 34 (1997), pp. 1072–1092.
- [3] K.-Y. CHEN, K.-A. FENG, Y. KIM, AND M.-C. LAI, *A note on pressure accuracy in immersed boundary method for Stokes flow*, J. Comput. Phys., 230 (2011), pp. 4377–4383.
- [4] F. H. HARLOW AND J. E. WELSH, *Numerical calculation of time-dependent viscous incompressible flow of fluid with a free surface*, Phys. Fluids, 8 (1965), pp. 2181–2189.
- [5] D. GOLDSTEIN, R. HANDLER, AND L. SIROVICH, *Modeling a no-slip flow boundary with an external force field*, J. Comput. Phys., 105 (1993), pp. 354–366.
- [6] K. H. DE HAAS, C. BLOM, D. VAN DEN ENDE, M. H. G. DUTS, AND J. MELLEMA, *Deformation of giant lipid bilayer vesicles in shear flow*, Phys. Rev. E, 56 (1997), pp. 7132–7137.
- [7] Y. KIM AND M.-C. LAI, *Simulating the dynamics of inextensible vesicles by the penalty immersed boundary method*, J. Comput. Phys., 229 (2010), pp. 4840–4853.
- [8] S. R. KELLER AND R. SKALAK, *Motion of a tank-treading ellipsoidal particle in a shear flow*, J. Fluid Mech., 120 (1982), pp. 27–47.
- [9] V. KANTSLER AND V. STEINBERG, *Orientation and dynamics of a vesicle in tank-treading motion in shear flow*, Phys. Rev. Lett., 95 (2005), 258101.

- [10] M. KRAUS, W. WINTZ, U. SEIFERT, AND R. LIPOWSKY, *Fluid vesicles in shear flow*, Phys. Rev. Lett., 77 (1996), pp. 3685–3688.
- [11] Z. LI AND M.-C. LAI, *New finite difference methods based on IIM for inextensible interfaces in incompressible flows*, East Asian J. Appl. Math., 1 (2011), pp. 155–171.
- [12] M.-C. LAI AND C. S. PESKIN, *An immersed boundary method with formal second order accuracy and reduced numerical viscosity*, J. Comput. Phys., 160 (2000), pp. 705–719.
- [13] M.-C. LAI, Y.-H. TSENG, AND H. HUANG, *An immersed boundary method for interfacial flow with insoluble surfactant*, J. Comput. Phys., 227 (2008), pp. 7279–7293.
- [14] H. NOGUCHI AND G. GOMPPER, *Shape transitions of fluid vesicles and red blood cells in capillary flows*, Proc. Natl. Acad. Sci. USA, 102 (2005), pp. 14159–14164.
- [15] J. B. PEROT, *An analysis of the fractional method*, J. Comput. Phys., 108 (1993), pp. 51–58.
- [16] C. S. PESKIN, *The immersed boundary method*, Acta Numer., 11 (2002), pp. 479–517.
- [17] C. POZRIKIDIS, *The axisymmetric deformation of a red blood cell in uniaxial straining Stokes flow*, J. Fluid Mech., 216 (1990), pp. 231–254.
- [18] J. PETERS, V. REICHEL, AND A. REUSKEN, *Fast iterative solvers for discrete Stokes equations*, SIAM J. Sci. Comput., 27 (2005), pp. 646–666.
- [19] E. M. SAIKI AND S. BIRINGEN, *Numerical simulation of a cylinder in uniform flow: Application of a virtual boundary method*, J. Comput. Phys., 123 (1996), pp. 450–465.
- [20] M. J. STEVENS, *Coarse-grained simulations of lipid bilayers*, J. Chem. Phys., 121 (2004), pp. 11942–11948.
- [21] G. W. SCHMID-SCHONBEIN, Y. Y. SHIH, AND S. CHIEN, *Morphometry of human leukocytes*, Blood, 56 (1980), pp. 866–875.
- [22] J. S. SOHN, Y.-H. TSENG, S. LI, A. VOIGT, AND J. S. LOWENGRUB, *Dynamics of multicomponent vesicles in a viscous fluid*, J. Comput. Phys., 229 (2010), pp. 119–144.
- [23] J. C. STRIKWERDA, *An iterative method for solving finite difference approximations to the Stokes equations*, SIAM J. Numer. Anal., 21 (1984), pp. 447–458.
- [24] K. TAIRA AND T. COLONIUS, *The immersed boundary method: A projection approach*, J. Comput. Phys., 225 (2007), pp. 2118–2137.
- [25] S. K. VEERAPANENI, D. GUEYFFIER, D. ZORIN, AND G. BIROS, *A boundary integral method for simulating the dynamics of inextensible vesicles suspended in a viscous fluid in 2D*, J. Comput. Phys., 228 (2009), pp. 2334–2353.
- [26] S. K. VEERAPANENI, Y.-N. YOUNG, P. M. VLAHOVSKA, AND J. BLAWZDZIEWICZ, *Dynamics of a compound vesicle in shear flow*, Phys. Rev. Lett., 106 (2011), 158103.
- [27] X. YANG, X. ZHANG, Z. LI, AND G.-W. HE, *A smoothing technique for discrete delta functions with application to immersed boundary method in moving boundary simulations*, J. Comput. Phys., 228 (2009), pp. 7821–7836.
- [28] H. ZHOU AND C. POZRIKIDIS, *Deformation of liquid capsules with incompressible interfaces in simple shear flow*, J. Fluid Mech., 283 (1995), pp. 175–200.